Inorg. Chem. **2006**, *45*, 4685–4694

Evaluation of Electron-Withdrawing Group Effects on Heme Binding in Designed Proteins: Implications for Heme *a* in Cytochrome *c* Oxidase

Jinyou Zhuang,[†] Jennifer H. Amoroso,[†] Ryan Kinloch,[‡] John H. Dawson,[‡] Michael J. Baldwin,[§] and Brian R. Gibney*[,†]

Department of Chemistry, Columbia University, 3000 Broadway, New York, New York 10027, Department of Chemistry and Biochemistry, University of South Carolina, Columbia, South Carolina 29208, and Department of Chemistry, University of Cincinnati, Cincinnati, Ohio 45221

Received January 14, 2006

Heme *a*, the metalloporphyrin cofactor unique to cytochrome *c* oxidases, differs from the more common heme *b* by two chemical modifications, a C-2 hydroxyethylfarnesyl group and a C-8 formyl group. To elucidate a role of the C-8 formyl group, we compare the heme affinity, spectroscopy, and electrochemistry of a heme *a* mimic, Fe(diacetyldeuterioporphyrin IX) or Fe(DADPIX), with heme *b*, Fe(protoporphryrin IX) or Fe(PPIX), incorporated into a designed heme protein. The $[\Delta 7\text{-H3m}]_2$ protein ligand, or maquette, selected for this study contains two equivalent bis-(3-methyl-L-histidine) heme binding sites within a four-α-helix bundle scaffold. The spectroscopic data on Fe(PPIX) and Fe(DADPIX) bound to $[\Delta 7\text{-H3m}]_2$ demonstrate that these complexes are excellent synthetic analogues for natural cytochromes *b* and *a*, respectively. Comparison of the spectroscopic, electrochemical, and equilibrium thermodynamic data measured for the Fe(PPIX)-$[\Delta 7\text{-H3m}]_2$ maquette with the previously reported Fe(PPIX)-$[\Delta 7\text{-His}]_2$ complex demonstrates that changing the heme axial ligands to 3-methyl-L-histidine from L-histidine does not alter the resulting heme protein properties significantly in either oxidation state. Heme binding studies demonstrate that $[\Delta 7\text{-H3m}]_2$ binds two ferrous Fe(DADPIX) or Fe(PPIX) moieties with similar dissociation constant values. However, in the ferric state, the data show that $[\Delta 7\text{-H3m}]_2$ only binds a single Fe(DADPIX) and that one 2500-fold weaker than oxidized Fe(PPIX). The data demonstrate that the 4.6 kcal mol^{-1} weakened affinity of $[\Delta 7\text{-H3m}]_2$ for oxidized Fe(DADPIX) results in the majority of the 160 mV, 3.7 kcal mol^{-1}, positive shift in the heme reduction potential relative to Fe(PPIX). These data indicate that a role of the formyl group on heme *a* is to raise the iron reduction potential, thus making it a better electron acceptor, but that it does so by destabilizing the affinity of bis-imidazole sites for the ferric state.

Introduction

Cytochrome *c* oxidase (CcO), [E.C. 1.9.3.1], is the terminal enzyme in aerobic metabolism that catalyses the four electron−four proton reduction of dioxygen with the pumping of four protons across the inner mitochrondrial membrane.[1] CcO contains an electron-transfer chain, composed of a binuclear Cu_A site and a bis-histidine-ligated low-spin heme *a*, which delivers reducing equivalents from water-soluble cytochrome *c* to the buried catalytic site, containing a heterobinuclear heme a_3−CuB site. The porphyrin cofactor of hemes $a + a_3$ is unique to CcO and is biosynthesized from the more prevalent heme *b*, Fe(protoporphyrin IX) or Fe(PPIX).[2] Figure 1 shows a comparison of the structures of heme *b* and heme *a* that illustrates the chemical modifications to the porphyrin peripheral architecture between these two heme macrocycles, the oxidation of the C-8 methyl into a formyl group, and the conversion of the vinyl group at

* To whom correspondence should be addressed. E-mail: brg@chem.columbia.edu. Phone: (212) 854-6346. Fax: (212) 932-1289.
[†] Columbia University.
[‡] University of South Carolina.
[§] University of Cincinnati.

(1) (a) Iwata, S.; Ostermeier, C.; Ludwig, B.; Michel, H. *Nature* **1995**, *376*, 660−669. (b) Babcock, G. T.; Wikström, M. *Nature* **1992**, *356*, 301−309. (c) Brzezinski, P. *Biochemistry* **1996**, *35*, 5611−5615. (d) Farver, O.; Einarsdóttir, Ó.; Pecht, I. *Eur. J. Biochem.* **2000**, *267*, 950−954. (e) García-Horsman, J. A.; Barquera, B.; Rumbley, J.; Ma, J.; Gennis, R. B. *J. Bacteriol.* **1994**, *176*, 5587−5600.
(2) (a) Nobrega, M. P.; Nobrega, F. G.; Tzagoloff, A. *J. Biol. Chem.* **1990**, *265*, 14220−14226. (b) Saiki, T.; Mogi, T.; Ogura, K.; Anraku, Y. *J. Biol. Chem.* **1993**, *268*, 26041−26044.

10.1021/ic060072c CCC: $33.50 © 2006 American Chemical Society
Published on Web 05/12/2006

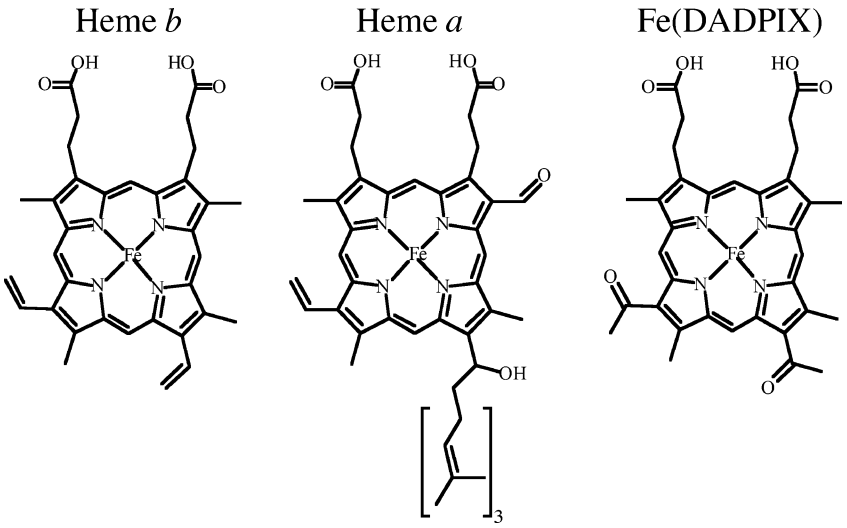

Figure 1. Chemical structures of heme *b* and heme *a* showing the C-8 formyl and C-2 hydroxyethylfarnesyl substitutents along with Fe(DADPIX).

C-2 into a hydroxyethylfarnesyl side chain. Despite significant advances in the understanding of the biosynthesis of heme *a* and CcO,[3] little is known as to the roles of these heme *a* side chains in the electron transfer and dioxygen reactivity of CcO.

The constructive methodology of de novo heme protein design[4] is elucidating fundamental structure−function relationships of natural heme proteins including CcO.[5] This approach to molecular design and synthetic biology[6] has afforded a variety of novel heme proteins as spectroscopic, electrochemical, and structural[7] bioinorganic model complexes for natural proteins involved in biological electron transfer,[8] oxygen transport,[9] and redox catalysis.[10] These water-soluble model systems have shown particular utility in revealing the key bioenergetic principles of heme-induced protein folding[11] and heme electrochemical function relevant to natural redox protein engineering.[12]

We are utilizing designed heme protein maquettes,[13] that is, peptide-based heme coordination complexes, to evaluate the factors governing the structure−function relationships of natural heme proteins such as CcO.[14] Using an analysis of the coordination equilibria involved in ferrous and ferric heme affinity, we are delineating the roles of various factors on heme protein electrochemistry in these simplified model systems. We have designed a four-α-helix bundle scaffold, $[\Delta 7\text{-}H_{10}I_{14}I_{21}]_2$ or $[\Delta 7\text{-His}]_2$, and determined its absolute affinity for ferric and ferrous heme at its pair of bis-His heme binding sites.[14] In addition, we have used this protein scaffold to expand the diversity of coordination motifs used in designed heme proteins beyond the typical bis-His ligated *b*-type cytochrome models to include bis-pyridyl and mono-histidine-ligated heme protein maquettes.[9,15]

Herein, we investigate the role of the electron-withdrawing C-8 formyl substitutent on heme *a*, the heme found exclusively in CcO, on heme affinity, and redox activity. Incorporation of Fe(2,4-diacetyldeuterioporphyrin IX),[16] Fe(DADPIX) structure in Figure 1, into a heme protein maquette with two bis-(3-methyl-L-histidine) heme binding sites, $[\Delta 7\text{-H3m}]_2$, generates a protein−ligand-based synthetic analogue for the electron-transfer cofactor heme *a* in CcO. In addition, a comparison of the ferric and ferrous heme affinities and the resulting electrochemistry of Fe(PPIX) and Fe(DADPIX) bound to $[\Delta 7\text{-H3m}]_2$ demonstrate a role of the acetyl groups in raising the iron reduction potential by weakening the affinity of the bis-imidazole site for the heme iron. These data support the proposal that one role of the electron-withdrawing formyl group on heme *a* is to raise the heme iron reduction potential and indicate that this elevation is done in large part by destabilization of the ferric state.

(3) (a) Carr, H. S.; Winge, D. R. *Acc. Chem. Res.* **2003**, *36*, 309−316. (b) Barros, M. H.; Nobrega, F. G.; Tzagoloff, A. *J. Biol. Chem.* **2002**, *277*, 9997−10002. (c) Barros, M. H.; Tzagoloff, A. *FEBS Lett.* **2002**, *516*, 119−123. (c) Brown, K. R.; Allan, B. M.; Do, P.; Hegg, E. L. *Biochemistry* **2002**, *41*, 10906−10913. (d) Brown, K. R.; Brown, B. M.; Hoagland, E.; Manye, C. L.; Hegg, E. L. *Biochemistry* **2004**, *43*, 8616−8624.

(4) (a) Reedy, C. J.; Gibney, B. R. *Chem. Rev.* **2004**, *104*, 589−604. (b) Lombardi, A.; Nastri, F.; Pavone, V. *Chem. Rev.* **2001**, *101*, 3165−3190.

(5) (a) Gibney, B. R.; Isogai, Y.; Reddy, K. S.; Rabanal, F.; Grosset, A. M.; Moser, C. C.; Dutton, P. L. *Biochemistry*, **2000**, *39*, 11041−11049. (b) Xu, Z.; Farid, R. S. *Protein Sci.* **2001**, *10*, 236−249.

(6) (a) Benner, S. A. *Nature* **2003**, *421*, 118. (b) Benner, S. A.; Sismore, A. M. *Nature Rev. Genet.* **2005**, *6*, 533−543.

(7) (a) Ghirlanda, G.; Osyczka, A.; Liu, W.; Antolovich, M.; Smith, K. M.; Dutton, P. L.; Wand, A. J.; DeGrado, W. F. *J. Am. Chem. Soc.* **2004**, *126*, 8141−8147. (b) Huang, S. S.; Koder, R. L.; Lewis, M. L. Wand, A. J.; Dutton P. L. *Proc. Natl. Acad. Sci., U.S.A.* **2004**, *101*, 5536−5541. (c) Rosenblatt, M. M.; Wang, J.; Suslick, K. S. *Proc. Natl. Acad. Sci., U.S.A.* **2003**, *100*, 13140−13145.

(8) (a) Sharp, R. E.; Moser, C. C.; Rabanal, F.; Dutton, P. L. *Proc. Natl. Acad. Sci. U.S.A.* **1998**, *95*, 10465−10469. (b) Rau, H. K.; DeJonge, N.; Haehnel, W. *Proc. Natl. Acad. Sci. U.S.A.* **1998**, *95*, 11526.-11530.

(9) Zhuang, J.; Amoroso, J. H.; Kinloch, R.; Dawson, J. H.; Baldwin, M. J.; Gibney, B. R. *Inorg. Chem.*, **2004**, *43*, 8218−8220.

(10) Moffet, D. A.; Certain, K. L.; Smith, A. J.; Kessel, A. J.; Beckwith, K. A.; Hecht, M. H. *J. Am. Chem.* Soc. **2000**, *122*, 7612−7613.

(11) Benson, D. R. Hart, B. R.; Zhu, X.; Doughty, M. B. *J. Am. Chem. Soc.* **1995**, *117*, 8502−8510.

(12) Gibney, B. R.; Dutton, P. L. *Adv. Inorg. Chem.* **2001**, *51*, 409−455.

(13) Robertson, D. E.; Farid, R. S.; Moser, C. C.; Urbauer, J. L.; Mulholland, S. E.; Pidikiti, R.; Lear, J. D.; Wand, A. J.; DeGrado, W. F.; Dutton, P. L. *Nature* **1994**, *368*, 425−432.

(14) Reedy, C. R. Kennedy, M. L.; Gibney, B. R. *Chem. Commun.* **2003**, 570−571.

(15) Privett, H. K.; Reedy, C. J.; Kennedy, M. L.; Gibney, B. R. *J. Am. Chem. Soc.*, **2002**, *124*, 6828−6829.

(16) Caughey, W. S.; Fujimoto, W. Y.; Johnson, B. P. *Biochemistry* **1966**, *5*, 3830−3843.

Materials and Methods

Reagents. Fmoc-protected amino acids were obtained from Bachem. HBTU, *O*-(1*H*-benzotriazole-1-yl)-*N*,*N*,*N*′,*N*′-tetramethyluronium hexafluorophosphate, was purchased from Qbiogene. Guanidine hydrochloride (8 M) was used as received from Pierce. All other chemicals and solvents were reagent grade.

Preparation of Peptides: General Procedure. The peptide ligand was synthesized on a continuous-flow Applied Biosystems Pioneeer solid-phase synthesizer using the Fmoc/^{t}Bu protection strategy[17] with PAL-PEG-PS resin (0.20 mmol g^{-1} loading) at 0.2 mmol scale. Single extended coupling cycles (60 min) with HBTU/DIEA activation chemistry were employed for all amino acids. The side chain protecting groups used are as follows. ^{t}Boc (Lys, His), O^{t}Bu (Glu), Trt (Cys), and Pbf (Arg). After peptide assembly, the N-terminus was manually acetylated followed by thorough washing with DMF, MeOH, and CH_2Cl_2. The peptide was cleaved from the resin and simultaneously deprotected using 90:8:2 (v/v/v) trifluoroacetic acid/ethanedithiol/water for 3 h. Crude peptide was precipitated and triturated with cold ether, dissolved in water (0.1% v/v TFA), lyophilized, and purified to homogeneity by reversed-phase C_{18} HPLC using aqueous−acetonitrile gradients containing 0.1% (v/v) TFA. The N-terminal cysteine residue of the purified peptide was air-oxidized to the symmetric disulfide in 100 mM ammonium carbonate buffer, pH 9.5 (5 h). After lyophilization, the identities of the resulting di-α-helical disulfide-bridged peptide was confirmed with matrix assisted laser desorption mass spectrometry.

Solution Molecular Weight Determination. Sedimentation equilibrium analytical ultracentrifugation analysis was performed on a Beckman XL-I analytical ultracentrifuge operating at 25 000 rpm and 4 °C.[18] Initial peptide concentrations ranged from 6 to 18 μM di-α-helical monomer in 20 mM KP_i, 100 mM KCl (pH 8.0). Partial specific volumes for the peptides were calculated from the residue-weighted average of the amino acid sequence using the method of Cohn and Edsall.[19] The partial specific volume of 3-methyl-L-histidine was estimated to be equivalent to that of L-histidine. The estimated partial specific volume, $\bar{\nu}$ value, was 0.7567 mL g^{-1}. The density, ρ, of the solvent buffer was 1.0509 g mL^{-1} (20 mM KP_i, 100 mM KCl, pH 8.0) as calculated using Sedenterp. The radial distribution absorbance scan data were fit to a single exponential using WinNonlin. The bouyant molecular weight, M_b, was converted to the average molecular weight of the molecular species in solution, M_r, with the following relationship:

$$M_b = M_r(1 - \bar{\nu}\rho)$$

Circular Dichroism Spectropolarimetry. Circular dichroism spectra were recorded on an AVIV 215 spectropolarimeter using rectangular quartz cells of 0.2 and 1.0 cm path length with a 5 s averaging time. Thermal control was maintained by a thermoelectric module with a ThermoNeslab M25 refrigerated recirculating water bath as a heat sink. Peptide concentrations in 20 mM KP_i, 100 KCl, pH 8.0 buffer were between 1 and 10 μM (four-helix bundle) as determined spectrophotometrically using $\epsilon_{280} = 5600$ M^{-1} cm^{-1} $helix^{-1}$ for Trp.[20]

Denaturation Studies. Peptide denaturation curves at 25 °C in 20 mM KP_i, 100 KCl, pH 8.0 buffer were fit to a dimer folded to two monomer unfolded equilibrium[21] using a nonlinear least squares routine in KaleidaGraph 3.6.

$$\text{fraction folded} = 1 - (\exp(-\Delta G_{unf}/RT)/4P)[(1 + 8P/\exp(-\Delta G_{unf}/RT))^{1/2} - 1]$$

where P is the molar concentration of total monomeric protein and $\Delta G_{unf} = \Delta G^{H_2O} - m$[Gdn·HCl], m is the cosolvation term which is a measure of the cooperativity of the transition and [denaturant] is the concentration of denaturant (M).

UV−Vis Spectroscopy. UV−visible spectra were recorded on Varian Cary 100 or Bio50 spectrophotometers using quartz cells of 0.1, 0.2, 1.0, and 10 cm path length. The concentrations of peptide in 20 mM KP_i, 100 KCl, pH 8.0 buffer were determined spectrophotometrically using ϵ_{280} of 5600 M^{-1} cm^{-1} per helix.

Heme Affinity Studies: Ferric Porphyrins. Freshly prepared DMSO solutions of hemin or Fe(DADPIX)Cl were added in 0.1 equiv aliquots to peptide solutions (20 mM KP_i, 100 mM KCl, pH 8.0) with 10 min equilibration between additions. The dissociation constant, K_d, values were obtained from fitting the absorbance at λ_{max}^{ox} plotted against [heme]/[four-helix bundle] according to an equation for two independent binding sites. Control experiments without peptide present were used to obtain the extinction coefficient for unbound hemin and Fe(DADPIX) used in the nonlinear least-squares fitting analysis of heme affinity.

Heme Affinity Studies: Ferrous Porphyrins. A freshly prepared DMSO solution of hemin or Fe(DADPIX)Cl was added in 0.1 equiv aliquots through a septum into anaerobic peptide solutions (20 mM KP_i, 100 mM KCl, pH 8.0) with 10 min equilibration between additions. The samples were maintained at a reducing potential by addition of sodium dithionite prior to the start of the titration. The K_d values were obtained from fitting the absorbance at λ_{max}^{red} plotted against [heme]/[four-helix bundle] according to an equation for two independent binding sites.

Magnetic Circular Dichroism Spectroscopy. The MCD spectra of the oxidized and reduced heme proteins dissolved in 20 mM KP_i, 100 KCl, pH 8.0 buffer were obtained at 4 °C using a Jasco J600 spectopolarimeter equipped with a Jasco MCD-1B electromagnet operated at a magnetic field of 1.41 T. Ferrous samples were generated under N_2 in a rubber septum sealed cuvette (1 or 0.5 cm) by adding a few grains of solid sodium dithionite to the ferric sample or by titrating the ferric sample with an aqueous solution of sodium dithionite (23 mg/mL). Formation of ferrous samples was monitored spectrophotometrically using a Varian Cary 400 spectrophotometer.

Preparation of Fe(DADPIX)(Im)$_2$. A ferric Fe(DADPIX) solution (400 μg of heme in 400 μL of DMSO) was diluted with a 1:1 mixture of methylene chloride and DMSO. The resulting DADPIX solution was titrated with 1-methylimidazole, and formation of the ferric bis-imidazole complex was monitored spectrophotometrically using a Varian 400 spectrophotometer. The ferrous bis-imidazole sample was prepared by treatment with solid sodium dithionite as described above.

Resonance Raman Spectroscopy. Raman spectra of oxidized and reduced heme peptide samples (100 μM heme protein in 20 mM KP_i, 100 KCl, pH 8.0 buffer) in 1 mm diameter capillary tubes were obtained at room temperature using a SPEX 1404 0.85 m double spectrometer with a liquid-N_2-cooled, 13.6 mm back-thinned SPEX Spectrum-1 CCD chip detector. Raman scattering was excited

(17) Carpino, L. A. *Acc. Chem. Res.* **1987**, *20*, 401−407.
(18) Laue, T. M.; Stafford III, W. F. *Annu. Rev. Biophys. Biomol. Struct.* **1999**, *28*, 75−100.
(19) Cohn, E. J.; Edsall, J. T. *Proteins, Amino Acids and Peptides*; Reinhold: New York, 1943; pp 445.
(20) Fasman, G. D. *Handbook of Biochemistry and Molecular Biology, Proteins I*; CRC Press: Boca Raton, FL, 1976.
(21) Mok, Y. K.; de Prat-Gay, G.; Butler, P. J.; Bycroft, M. *Protein Sci.* **1995**, *5*, 310−319.

by the 441.6 nm line (~30 mW at the sample) of a Kimmon IK series HeCd laser. Raman shifts were calibrated against the laser emission at 441.6 nm. Three separate data sets consisting of 25, 25, and 10 spectra with 120 s integration time were averaged (weighted by number of spectra) after a linear baseline correction was applied to each of the three data sets.

Heme Redox Potentiometry. Chemical redox titrations were performed in an anaerobic cuvette equipped with a platinum working and a calomel reference electrode at 22 °C.[22] Ambient potentials (measured against the standard hydrogen electrode) were adjusted by addition of aliquots (<1 μL) of sodium dithionite or potassium ferricyanide. Titrations were performed in 20 mM potassium phosphate, 100 mM KCl, pH 8.0. Electrode−solution mediation was facilitated by the following mediators at 10 μM concentration: methyl viologen, benzyl viologen, anthroquinone-2-sulfonate, anthroquinone-2,6-disulfonate, 2-hydroxy-1,4-naphthoquinone, indigotrisulfonate, duroquinone, 5-hydroxy-1,4-naphthoquinone, 1,4-naphthoquinone, phenazine ethosulfate, phenazine methosulfate, 2,6-dimethyl benzoquinone, 1,2-naphthoquinone, 2-methyl-1,4-benzoquinone, 1,2-naphthoquinone-4-sulfonic acid, and resorufin. After equilibration at each potential, the optical spectrum was recorded. Heme reduction was followed by the increase in either γ-band absorption (426 and 450 nm) relative to a baseline wavelength (800 nm). Spectral intensity was plotted against potential, and the data were fit to either a single or a pair of Nernst equations of equal weight with $n = 1.0$ (fixed).

Results

Experimental Design. The midpoint reduction potential of heme bound to a protein, E_m^{bound}, is governed by the ratio of ferric and ferrous heme dissociation constant values, $K_d^{Fe(III)} / K_d^{Fe(II)}$, and the reduction potential of the unbound heme, E_m^{free}, as follows[23]

$$E_m^{bound} = E_m^{free} + (RT/nF) \ln[K_d^{Fe(III)}/K_d^{Fe(II)}] \quad (1)$$

$$\text{Protein} + \text{Heme} \rightleftharpoons \text{Heme}-\text{Protein} \quad (2)$$

$$K_d = [\text{Heme}][\text{Protein}]/[\text{Heme}-\text{Protein}] \quad (3)$$

We have measured the electrochemistry and absolute affinities of oxidized and reduced hemes for designed proteins in an effort to clarify the various contributors to ferric and ferrous heme affinity in natural heme proteins.[9,14] These thermodynamic data are crucial to a more complete understanding of heme protein structure−function relationships as heme binding is integral to protein folding,[24] and the resulting heme midpoint reduction potential provides the driving force for electron-transfer reactivity.[25] Furthermore, elucidation of the metal-binding thermodynamics using coordination chemistry methods provides the fundamental data necessary to evaluate the relative energetics between metal-ion binding and protein folding in the field of heme protein design.[26]

We have developed a truncated heme protein maquette scaffold, $[\Delta 7\text{-}H_{10}I_{14}I_{21}]_2$ or $[\Delta 7\text{-His}]_2$, whose absolute affinities for both the ferric and ferrous Fe(PPIX) have been accurately measured.[14] The $[\Delta 7\text{-His}]_2$ scaffold is composed of two disulfide-bridged di-α-helical monomers, each of which contains a single bis-His heme binding site. The determination of the absolute affinity of this bis-histidine $[\Delta 7\text{-His}]_2$ maquette for Fe(PPIX) in both oxidation states along with the coupled electrochemistry provides significant insight into the design of synthetic heme proteins. The ability to measure these thermodynamics is relatively rare among both natural and designed heme proteins. In the case of synthetic heme proteins,[1] most are only assayed in the ferric state without regard for the ferrous heme affinities, which leads to an incomplete view of the coordination equilibria of these heme proteins. The same is true in the case of natural heme protein scaffolds in which full thermodynamic analysis is often further complicated by tight heme binding or other biochemical issues, e.g., kinetic trapping of the heme moiety.[27]

In this study, we evaluate the affinity of a maquette scaffold for Fe(PPIX) and Fe(DADPIX), an analogue of heme *a*, in both the ferrous and ferric forms in order to describe the electrochemical differences between the resulting proteins. A novel maquette scaffold, $[\Delta 7\text{-H3m}]_2$, containing two bis-(3-methyl-L-histidine) heme binding sites is utilized for this study in our continuing efforts to extend the coordination spheres available for heme protein design.[9,15] The 3-methyl-L-histidine ligand was selected to evaluate if methylation at N^δ would interfere with heme coordination. In addition, the $[\Delta 7\text{-H3m}]_2$ scaffold provides a primary coordination sphere that more closely mimics the ligand *N*-methylimidazole, which is routinely used in thermodynamic and structural studies of iron porphyrin synthetic analogues in the place of imidazole which self-associates in solution.[23,28] Ultimately, the comparison of Fe(PPIX) binding to the $[\Delta 7\text{-H3m}]_2$ and the $[\Delta 7\text{-His}]_2$ scaffolds demonstrates that the binding thermodynamics of the 3-methyl-L-histidine and L-histidine scaffolds are similar, which shows that N^δ methylation does not adversely affect heme binding. Thermodynamic data on Fe(PPIX) and Fe(DADPIX) binding to $[\Delta 7\text{-H3m}]_2$ are used to evaluate the roles of electron-withdrawing groups such as the C-8 formyl group on heme *a* in CcO, on heme binding, and electrochemistry. These data are used to suggest individual roles for the C-8 formyl and the C-2 hydroxyethylfarnesyl groups on ferric and ferrous heme *a* affinity and electrochemistry in CcO.

Peptide Secondary Structure. Figure 2A presents the far-UV CD spectrum of $[\Delta 7\text{-H3m}]_2$ at 7.6 μM concentration in aqueous buffer, black trace, which is characteristic of an α-helical peptide (70% helical content) with minima at 208

(22) Dutton, P. L. *Methods Enzymol.* **1978**, *54*, 411−435.
(23) Nesset, M. J. M.; Shokhirev, N. V.; Enemark, P. D.; Jacobson, S. E.; Walker, F. A. *Inorg. Chem.*, **1996**, *35*, 5188−5200.
(24) (a) Bai, Y. W.; Sosnick, T. R.; Mayne, L.; Englander, S. W. *Science* **1995**, *269*, 192. (b) Telford, J. R.; Wittung-Stafshede, P.; Gray, H. B.; Winkler, J. R. *Acc. Chem. Res.* **1998**, *31*, 755.
(25) (a) Beratan, D. N.; Onuchic, J. N.; Winkler, J. R.; Gray, H. B. *Science* **1992**, *258*, 1740. (b) Page, C. C.; Moser, C. C.; Chen, X. X.; Dutton, P. L. *Nature* **1999**, *402*, 47.
(26) Bryson, J. W.; Betz, S. F.; Lu, H. S.; Suich, D. J.; Zhou, H. X. X.; O'Neil, K. T.; DeGrado, W. F. *Science* **1995**, *270*, 935−941.
(27) Wang, J.; Bieber Urbauer, R. J.; Urbauer, J. L.; Benson, D. R. *Biochem. Biophys. Res. Comm.* **2003**, *305*, 840−845.
(28) Collman, J. P.; Gagne, R. R.; Reed, C. A.; Robinson, W. T.; Rodley, G. A. *Proc. Natl. Acad. Sci. U.S.A.* **1974**, *71*, 1326−1329.

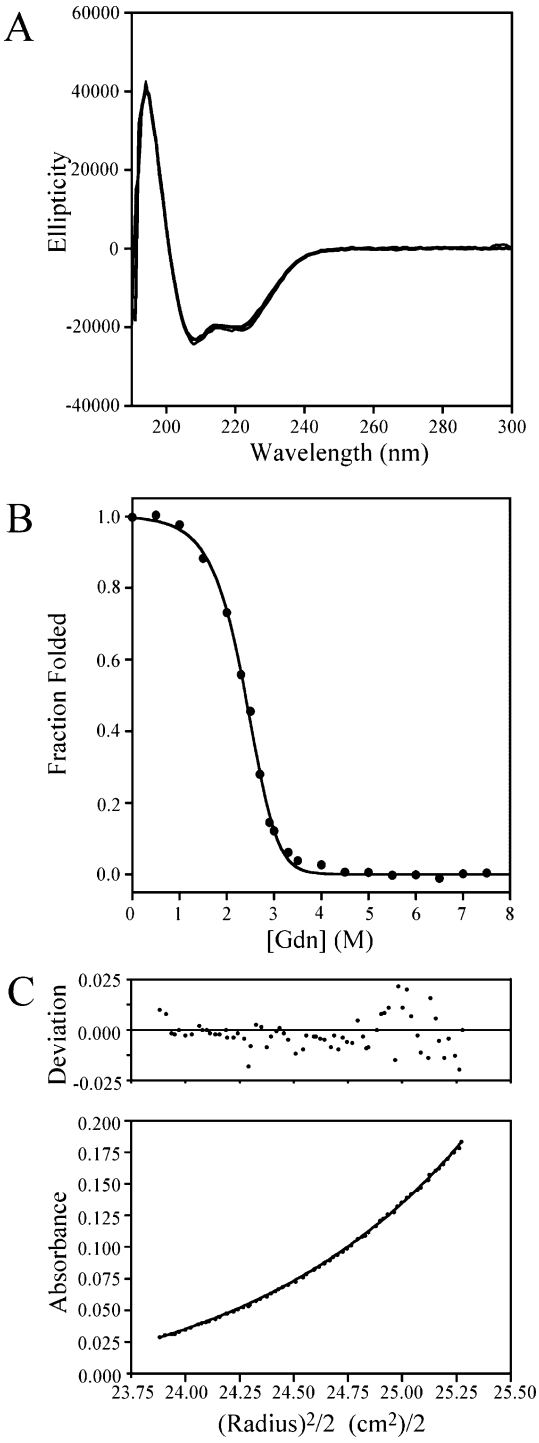

Figure 2. Biophysical characterization of the $[\Delta 7\text{-H3m}]_2$ maquette scaffold. (A) Circular dichroism spectrum of $[\Delta 7\text{-H3m}]_2$, black trace, and mono-Fe(DADPIX)-$[\Delta 7\text{-H3m}]_2$, blue trace, at 7.6 μM concentration. The minima at 208 and 222 nm and maxima at 196 nm indicate 70% and 72% helix content for the apo- and holo-proteins, respectively. (B) Isothermal chemical denaturation of the apo-protein scaffold at 7.6 μM concentration fit to an unfolded monomer−folded dimer equlibrium. The fit demonstrates a stability of −12.8 kcal/mol for the $[\Delta 7\text{-H3m}]_2$ helical bundle. (C) Sedimentation equilibrium analytical ultracentrifugation analysis of $[\Delta 7\text{-H3m}]_2$ using a Beckman XL-I ultracentrifuge. An 4.5 μM solution of $[\Delta 7\text{-H3m}]_2$ was centrifuged at 25 000 rpm for 24 h before data collection. The radial absorbance data at 280 nm (tryptophan absorbance) is fit to a single solution species with a 13.1 kDa solution molecular weight consistent with a dimer oligomerization state, i.e., four-α-helix bundle. The residuals to the fit are shown above the data. All experiments were performed in 20 mM KP_i, 100 KCl, pH 8.0 buffer.

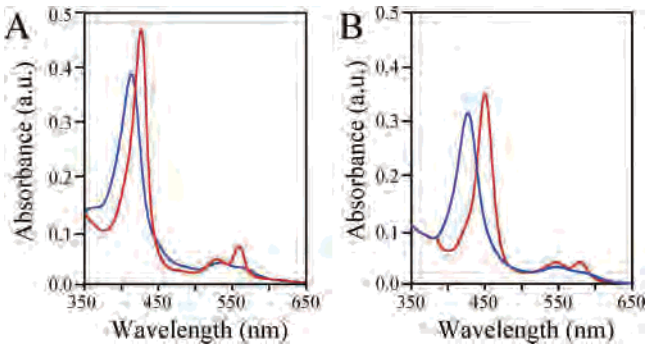

Figure 3. UV−vis spectra of the Fe(PPIX)- and Fe(DADPIX)-$[\Delta 7\text{-H3m}]_2$ complexes. (A) Optical spectra of Fe(PPIX)-$[\Delta 7\text{-H3m}]_2$ at 4.1 μM concentration in the ferric (blue) and ferrous (red) states. (B) Optical spectra of the ferric (blue) and ferrous (red) Fe(DADPIX)-$[\Delta 7\text{-H3m}]_2$ complex at 4.1 μM concentration. Spectra were recorded in 20 mM KP_i, 100 mM KCl, pH 8.0 buffer at 25 °C.

and 222 nm ($\pi \rightarrow \pi^*$ and n $\rightarrow \pi^*$ minima of α-helical systems, respectively).[29] The helix content of the peptide scaffold containing 3-methyl-L-histidine (70%) is slightly higher than that of the histidine prototype (67%) and its isomer the 1-methyl-L-histidine maquette (68%), suggesting that these amino acid changes do not alter the secondary structure significantly. Figure 2A also shows the far-UV CD spectrum of Fe(DADPIX)-$[\Delta 7\text{-H3m}]_2$ at 7.6 μM concentration, blue trace, which indicates 72% helical content. Thus, the incorporation of the heme macrocycle does not alter the secondary structure of the protein significantly. Chemical denaturation studies with guanidine hydrochloride, Figure 2B, demonstrate that $[\Delta 7\text{-H3m}]_2$ is stable in the apo-form, $\Delta G^{H_2O} = -12.8$ kcal/mol at 298 K ($[\text{Gdn}\cdot\text{HCl}]_{1/2}$ value of 2.4 M; *m* value of 2.5). Thus, the protein folds into a stable helical fold in solution, as designed.

Peptide Oligomerization State. The oligomerization state of the disulfide-bridged di-α-helical peptide was determined using sedimentation equilibrium analytical ultracentrifugation over the protein concentration range of 1−18 μM. Figure 2C shows the radial distribution of the tryptophan absorbance at 280 nm for *apo*-$[\Delta 7\text{-H3m}]_2$ at a protein concentration of 4.5 μM. The fit to the data demonstrates a solution molecular weight of 13.1 kDa, indicative of a dimeric oligomerization state for $[\Delta 7\text{-H3m}]_2$. Together with the CD results, these data indicate that the protein sequence folds into the desired four-α-helix bundle scaffold.

Fe(PPIX) Binding. Figure 3A presents the optical spectra of ferric and ferrous iron(protoporphyrin IX) bound to $[\Delta 7\text{-H3m}]_2$ at 4.1 μM concentration. The oxidized heme was incorporated into $[\Delta 7\text{-H3m}]_2$ in 20 mM KP_i, 100 KCl, pH 8.0 buffer and followed by UV−visible spectroscopy. Similar to the bis-His maquette, Fe(PPIX)-$[\Delta 7\text{-His}]_2$,[14] the spectrum of Fe(PPIX) bound to $[\Delta 7\text{-H3m}]_2$ possess a Soret maximum at 412 nm ($\epsilon = 123$ mM^{-1} cm^{-1}) with α/β bands at 535 nm ($\epsilon = 13.0$ mM^{-1} cm^{-1}). Reduction of the ferric Fe(PPIX)-$[\Delta 7\text{-H3m}]_2$ with a minimal quantity of sodium dithionite results in formation of the ferrous Fe(PPIX)-$[\Delta 7\text{-H3m}]_2$ complex, as evinced by a Soret maximum at 427 nm ($\epsilon =$

(29) Nakanishi, K.; Berova, N.; Woody, R. W. *Circular dichroism of peptides*; VCH: New York, 1994; p 570.

191 mM^{-1} cm^{-1}) with distinct α/β bands at 529 nm (ϵ = 18.0 mM^{-1} cm^{-1}) and 560 nm (ϵ = 33.2 mM^{-1} cm^{-1}). The resolution of the α/β bands in the reduced state is indicative of the designed bis-imidazole coordination that yields a low-spin ferrous heme due to the strong ligand field.[30] These spectroscopic data indicate that methylation of the imidazole nitrogen not involved in heme coordination, N^{δ} of histidine, results in no significant alteration of the bound heme spectroscopic properties.

Incorporation of Fe(DADPIX). Figure 3B shows the optical spectra of oxidized and reduced Fe(DADPIX) bound to $[\Delta 7\text{-H3m}]_2$ at 4.1 μM concentration. The ferric Fe(DADPIX) cofactor was incorporated under aerobic conditions and followed by UV−visible spectroscopy. The spectrum of ferric Fe(DADPIX) exhibits a Soret λ_{max} at 426 nm (ϵ of 89 mM^{-1} cm^{-1}) and is indicative of iron coordination but is slightly red-shifted relative to the of 420−425 nm λ_{max} of heme a + heme a_3 in CcO[31] and the λ_{max} value of 421 nm observed in a previous bis-His heme a maquette, [heme a − H10A24]$_2$.[5a] Dithionite reduction to ferrous Fe(DADPIX)-$[\Delta 7\text{-H3m}]_2$ results in a shift of the Soret maximum to 450 nm (ϵ of 110 mM^{-1} cm^{-1}) with distinct α/β bands at 545 and 578 nm (ϵ of 12.6 and 13.3 mM^{-1} cm^{-1}, respectively) indicative of bis-imidazole coordination. As observed for the ferric oxidation state, the optical properties of ferrous Fe(DADPIX)-$[\Delta 7\text{-H3m}]_2$ are slightly red-shifted relative to CcO, λ_{max} values of 440−445 nm,[31] and the heme a maquette, λ_{max} 441 nm.[5a] The slight spectral differences between Fe(DADPIX) and heme a bound to bis-imidazole binding sites in two maquette scaffolds are likely a result of the presence of the two electron-withdrawing acetyl groups on Fe(DADPIX) relative to the single formyl group on heme a.

Resonance Raman Characterization of Fe(PPIX)- and Fe(DADPIX)-$[\Delta 7\text{-H3m}]_2$. Since resonance Raman (rR) spectroscopy of heme proteins[32] is responsive to oxidation state, spin-state, and axial ligand changes, the rR spectra of ferric and ferrous Fe(PPIX)- and Fe(DADPIX)-$[\Delta 7\text{-H3m}]_2$ were collected and analyzed. Figure 4A shows the resonance Raman (rR) spectrum of Fe(PPIX)-$[\Delta 7\text{-H3m}]_2$ in both oxidation states. In the ferric state shown in the blue trace, the oxidation state marker band, ν_4, is at 1373 cm^{-1} and the spin state marker bands, ν_2, ν_3, and ν_{10}, are at 1587, 1504, and 1641 cm^{-1}, respectively. These ν_2, ν_3, ν_4, and ν_{10} band positions are nearly identical to those observed for ferric bis-histidine ligated cyt b_5, 1585, 1506, 1374, and 1640 cm^{-1} and Fe(III)(PPIX)(Im)$_2$, 1579, 1502, 1373, and 1640 cm^{-1}, which confirms the presence of a bis-imidazole ligated low-spin ferric heme, as designed.[33] In the ferrous form shown in red, the rR spectrum of $[\Delta 7\text{-H3m}]_2$ is also similar to those reported for ferrous cyt b_5 and Fe(II)(PPIX)(Im)$_2$. As

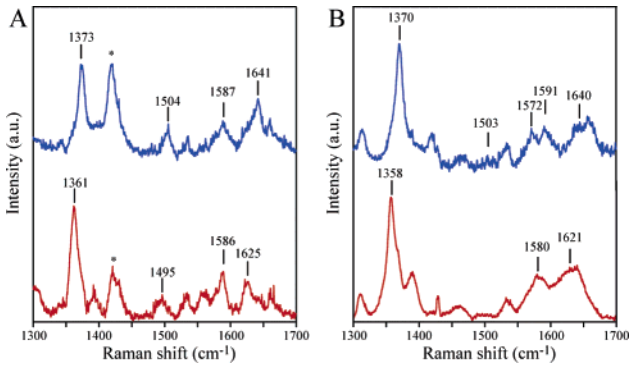

Figure 4. Resonance Raman spectroscopic characterization of Fe(PPIX)- and Fe(DADPIX)-$[\Delta 7\text{-H3m}]_2$ complexes. (A) Resonance Raman spectra of Fe(PPIX)-$[\Delta 7\text{-H3m}]_2$ recorded at 100 μM protein concentration in the oxidized (blue) and reduced (red) states. A vibrational band due to the DMSO used to incorporate the heme is noted with an asterisk. (B) Resonance Raman spectra of the Fe(DADPIX)-$[\Delta 7\text{-H3m}]_2$ complex recorded at 100 μM protein concentration in the oxidized (blue) and reduced (red) states. The positions and intensities of the spin-state marker bands, ν_3, ν_2, and ν_{10} are indicative of six-coordinate low-spin Fe(PPIX) and Fe(DADPIX) in both oxidation states.

expected upon reduction, the ν_4 oxidation state marker band in the rR spectrum of $[\Delta 7\text{-H3m}]_2$ shifts to lower frequency, 1361 cm^{-1}. Additionally, the spin state marker bands ν_2, ν_3, and ν_{10} shift to values of 1586, 1495, and 1625 cm^{-1}, respectively. The similarity of these values to those reported for cyt b_5 and Fe(II)(PPIX)(Im)$_2$ indicate that the maquette contains low-spin bis-imidazole-ligated ferrous hemes.[33] Figure 4B shows the rR spectra of ferric and ferrous Fe(DADPIX)-$[\Delta 7\text{-H3m}]_2$. Based on the observed similarities in the rR spectra of Fe(DADPIX)- and Fe(PPIX)-$[\Delta 7\text{-H3m}]_2$, we have assigned the oxidation-state marker band, ν_4, at 1370 cm^{-1} and the spin-state marker bands, ν_2, ν_3, and ν_{10}, at 1591, 1503, and 1640 cm^{-1}, respectively. In the reduced state (red trace), we assign the rR spectrum of Fe(DADPIX)-$[\Delta 7\text{-H3m}]_2$, as follows. The ν_4 oxidation-state marker band at 1358 cm^{-1} and the spin-state marker bands ν_2 and ν_{10} at 1580 and 1621 cm^{-1}, respectively. Since no rR spectral assignments of Fe(DADPIX) complexes are available in the literature, these assignments are tentative. However, the rR spectra of Fe(DADPIX)-$[\Delta 7\text{-H3m}]_2$ are similar to Fe(deuterioporphyrin IX)-substituted cytochrome b_5 which supports these assignments.[32b] Furthermore, the similarities between the rR spectra of Fe(DADPIX)- and Fe(PPIX)-$[\Delta 7\text{-H3m}]_2$ suggests that both contain low-spin bis-His coordinated irons.

Magnetic Circular Dichroism Characterization of Fe(PPIX)- and Fe(DADPIX)-$[\Delta 7\text{-H3m}]_2$. The magnetic circular dichroism (MCD) spectrum of a heme is sensitive to the iron spin state, oxidation state, and axial ligands.[34] MCD was used to confirm the designed coordination sphere of the iron in ferric and ferrous Fe(PPIX)- and Fe(DADPIX)-$[\Delta 7\text{-H3m}]_2$. The MCD spectrum of ferric and ferrous $[\Delta 7\text{-H3m}]_2$ in aqueous buffer (20 mM KP_i, 100 mM KCl, pH 8.0, 4 °C)

(30) Yu, L.; Xu, J.-X.; Haley, P. E.; Yu, C. A. *J. Biol. Chem.* **1987**, *262*, 1137−1143.
(31) Yonetani, T. *J. Biol. Chem.* **1961**, *236*, 1850−1856.
(32) (a) Spiro, T. G. *Biological Applications of Raman Spectroscopy*; Wiley-Interscience: New York, 1988; Vol. 1−3. (b) Spiro, T. G.; Strekas, T. C. *J. Am. Chem. Soc.* **1974**, *96*, 338−345. (c) Takahashi, S.; Wang, J.; Rousseau, D. L.; Ishikawa, K.; Yoshida, T.; Takeuchi, N.; Ikeda-Saito, M. *Biochemistry* **1994**, *33*, 5531−5538.d) Spiro, T. G.; Strong, J. D.; Stein, P. J. *J. Am. Chem. Soc.* **1979**, *101*, 2648−2655.
(33) (a) Kitagawa, T.; Sugiyama, T.; Yamano. T. *Biochemistry* **1982**, *21*, 1680−1686. (b) Adar, F. *Arch. Biochem. Biophys.* **1975**, *170*, 644−650.
(34) Cheek, J.; Dawson, J. H. In *The Porphyrin Handbook*; Academic Press: San Diego, 2000; Vol. 7, pp 339−369.

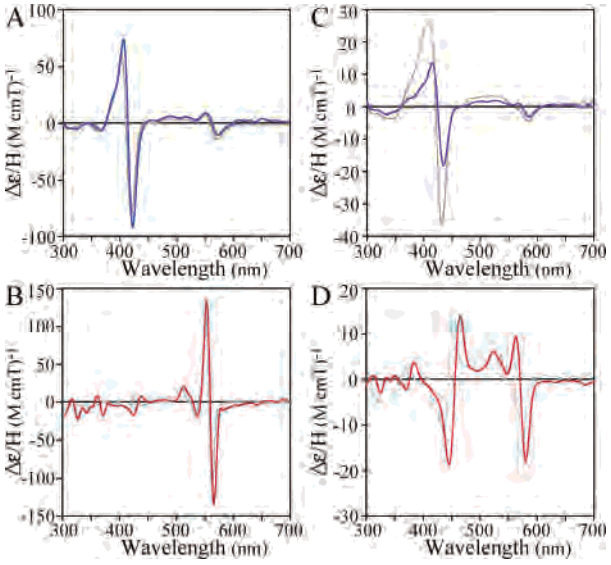

Figure 5. Magnetic circular dichroism spectra of the Fe(PPIX)- and Fe(DADPIX)-[Δ7-H3m]$_2$ complexes. MCD spectra of Fe(PPIX)-[Δ7-H3m]$_2$ in the ferric form (blue trace in A) and ferrous (red trace in B) forms. The MCD spectra of ferrous and ferric cytochrome b_5 is shown in gray for comparison. The MCD spectra of Fe(DADPIX) in the ferric (blue trace in C) and ferrous (red trace in D) forms. The MCD spectra of Fe(DADPIX) are shown in comparison to the bis-imidazole complex of Fe(DADPIX) (gray traces in C and D). The MCD data of cytochrome b_5 was replotted from ref 41.

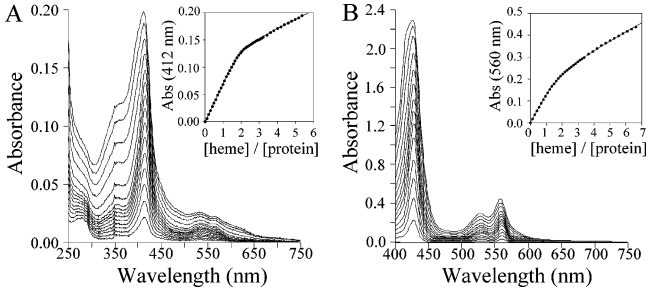

Figure 6. Analysis of the [Δ7-H3m]$_2$ affinity for Fe(PPIX) in the ferric and ferrous states performed using optical spectroscopy. (A) Titration of ferric Fe(PPIX) into a 790 nM [Δ7-H3m]$_2$ solution in a 1.0 cm quartz cell. The inset shows the absorption at 426 nm fit to a 2:1 Fe(III)(PPIX):[Δ7-H3m]$_2$ complex with a heme dissociation constants values of <1 nM and 70 nM. (B) Ferrous Fe(PPIX) titrated into a 6.2 μM [Δ7-H3m]$_2$ solution in a 1.0 cm quartz cell under anaerobic conditions. The inset shows the absorption at 560 nm, the α-band maximum, fit to a 2:1 Fe(II)(PPIX):[Δ7-H3m]$_2$ complex with a dissociation constant values of 20 nM and 4.0 μM. All samples were in 20 mM KP$_i$, 100 mM KCl, pH 8.0 buffer and allowed to equilibrate for 10 min prior to measurement on a Cary 100 spectrophotometer.

are shown as panels A and B of Figure 5, respectively. In both oxidation states, the MCD spectra of [Δ7-H3m]$_2$ demonstrate striking similarity to that of a natural bis-His ligated heme protein, cytochrome b_5, shown in gray for comparison. The near superposition of the MCD spectra (band shape, peak positions, and crossover points) between cyt b_5 and Fe(PPIX)-[Δ7-H3m]$_2$ demonstrate the presence of hexacoordinate low-spin hemes in the maquette. The MCD spectra for ferric and ferrous Fe(DADPIX)-[Δ7-H3m]$_2$ were collected and compared to the model complex Fe(DADPIX)-(Im)$_2$ since no natural counterpart is available. As shown in Figure 5C and D, the MCD spectra of Fe(DADPIX)-[Δ7-H3m]$_2$ is similar to those of Fe(DADPIX)(Im)$_2$ in the ferric and ferrous heme oxidation states, respectively. Thus, the ferric and ferrous MCD spectra of Fe(DADPIX)-[Δ7-H3m]$_2$ are consistent with the designed low-spin bis-(3-methyl-L-histidine) coordination.

Heme Affinity Studies of Fe(PPIX)-[Δ7-H3m]$_2$. The affinity of the protein ligand for Fe(PPIX) in each oxidation state was determined using titrations at a variety of protein concentrations. UV−visible spectroscopic titrations over peptide concentrations ranging from 50 nM to 6.2 μM in rectangular cells of 10 and 1 cm path length were used to determine the two individual heme dissociation constants, K_{d1} and K_{d2} values, of [Δ7-H3m]$_2$. Titrations of freshly prepared solutions of hemin, Fe(PPIX)Cl, in DMSO into aqueous solutions of [Δ7-H3m]$_2$ containing 20 mM KP$_i$, 100 mM KCl, pH 8.0 buffer were performed with gentle stirring. As observed with other protein maquettes containing Fe(PPIX),[14] the spectral changes indicate that oxidized heme equilibration is complete within 5 min. Figure 6A shows the ferric Fe(PPIX) titration data for a [Δ7-H3m]$_2$ concentration of 790 nM which clearly demonstrates the expected 2:1 heme-to-four-α-helix bundle stoichiometry. An analogous titration at 50 nM showed a single dissociation constant, $K_{d1}^{Fe(III)}$, value that was determined to be tighter than 1 nM. The inset in Figure 6A shows that the increase in absorbance at 412 nm fits well to a two independent heme per four helix bundle binding model with a second $K_{d2}^{Fe(III)}$ value of 70 nM when the first $K_{d1}^{Fe(III)}$ is fixed at < 1 nM. Figure 6B gives the ferrous Fe(PPIX) titration data for [Δ7-H3m]$_2$ at a concentration of 6.2 μM under anaerobic conditions. The inset to Figure 6B show formation of a 2:1 heme-to-four-α-helix bundle complex with a second $K_{d2}^{Fe(II)}$ value of 4.0 μM. An analogous titration at a protein concentration of 100 nM was used to evaluate the first dissociation constant, $K_{d1}^{Fe(II)}$, value of 20 nM for ferrous Fe(PPIX)-[Δ7-H3m]$_2$. The similarity of these ferrous and ferric K_d values to those of the histidine prototype, [Δ7-His]$_2$ (oxidized, $K_{d1}^{Fe(III)}$ is 140 pM and $K_{d2}^{Fe(III)}$ is 400 nM; reduced, $K_{d1}^{Fe(II)}$ is 42 nM and $K_{d2}^{Fe(II)}$ is 15 μM),[14] illustrates that methylation of the N$^{\delta}$ of histidine has only a relatively minor effect on heme affinity.

Heme Affinity Studies of Fe(DADPIX)-[Δ7-H3m]$_2$. The affinity of [Δ7-H3m]$_2$ for ferric and ferrous Fe(DADPIX) was determined using UV−vis titrations at protein concentrations from 50 nM to 50 μM. Freshly prepared solutions of Fe(DADPIX)Cl in DMSO were titrated into aqueous solutions of [Δ7-H3m]$_2$ with gentle stirring. Fe(DADPIX) incorporation was complete within 5 min, which is considerably faster than the 90 min required to bind heme *a* to a related maquette scaffold.[5a] Figure 7A shows the ferric Fe(DADPIX) titration data for [Δ7-H3m]$_2$ at a concentration of 1.34 μM in 20 mM KP$_i$, 100 mM KCl, pH 8.0 buffer. The data evince a 1:1 Fe(DADPIX)-to-four-α-helix bundle stoichiometry at this concentration. Analysis of the absorbance at 426 nm as a function of added Fe(DADPIX) with a heme binding model yields a $K_{d1}^{Fe(III)}$ value of 200 nM. Experimental attempts to determine the value of the second dissociation constant for ferric Fe(DADPIX), $K_{d2}^{Fe(III)}$, by titration at higher protein concentrations yielded only a weak

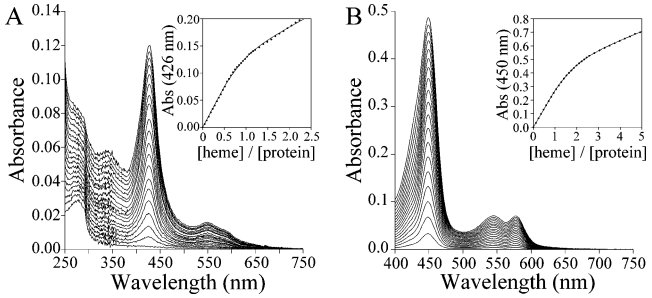

Figure 7. Thermodynamic analysis of the $[\Delta 7\text{-H3m}]_2$ affinity for ferric and ferrous Fe(DADPIX) followed by optical spectroscopy. (A) Fe(III)-(DADPIX) was titrated into a 1.34 μM solution of $[\Delta 7\text{-H3m}]_2$ in 20 mM KP_i, 100 mM KCl, pH 8.0 in a 1.0 cm quartz cell. The inset shows the absorption at 426 nm fit to a 1:1 Fe(DADPIX):$[\Delta 7\text{-H3m}]_2$ complex. (B) Ferrous Fe(DADPIX) was titrated into a 2.32 μM $[\Delta 7\text{-H3m}]_2$ solution in a 1.0 cm quartz cell under anaerobic conditions. The inset shows the absorption at 450 nm fit to a 2:1 Fe(DADPIX):$[\Delta 7\text{-H3m}]_2$ complex. All samples were equilibrated 10 min between additions prior to measurement on a Cary 100 spectrophotometer.

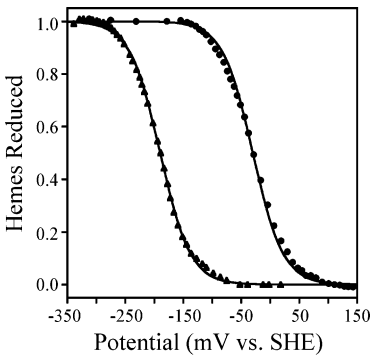

Figure 8. Spectroelectrochemical determination of the equilibrium midpoint reduction potentials for the Fe(PPIX)-$[\Delta 7\text{-H3m}]_2$ (▲) and Fe-(DADPIX)-$[\Delta 7\text{-H3m}]_2$ (●) heme protein maquettes at pH 8.0. The data are fit to single $N = 1$ Nernst curves with a midpoint reduction potentials of -190 ± 10 and -30 ± 10 mV vs SHE, respectively.

limit of 500 μM. Thus, $[\Delta 7\text{-H3m}]_2$ binds Fe(DADPIX) significantly weaker than Fe(PPIX) in the oxidized state. In the reduced state, the titration curve measured for Fe-(DADPIX) binding to $[\Delta 7\text{-H3m}]_2$ at a concentration of 2.3 μM shows formation of a tight 2:1 heme/four-helix bundle complex, as designed. Fits to data sets at a variety of concentrations indicate that the first ferrous Fe(DADPIX) dissociation constant, $K_{d1}^{Fe(II)}$, has a value of 37 nM, while the second $K_{d2}^{Fe(II)}$ has a value of 730 nM. These ferrous $K_{d1}^{Fe(II)}$ and $K_{d2}^{Fe(II)}$ values are close to those determined for Fe(PPIX) in the same scaffold, [Δ7-H3m]2, and suggest that the acetyl groups do not have major steric or electronic effects on Fe(II)−ligand bonding.

Redox Activity Comparison of Fe(PPIX)- and Fe-(DADPIX)-$[\Delta 7\text{-H3m}]_2$. Figure 8 shows the electrochemistry of Fe(PPIX)- and Fe(DADPIX)-$[\Delta 7\text{-H3m}]_2$ as evaluated using UV−visible spectroelectrochemistry. For monoheme-$[\Delta 7\text{-H3m}]_2$, the increase in the Fe(PPIX) Soret absorption at 426 nm due to iron reduction fits to an equilibrium midpoint reduction potential at pH 8, E_{m8} value, of -190 ± 10 mV vs SHE. Diheme-$[\Delta 7\text{-H3m}]_2$ demonstrates two individual heme reduction potentials, −170 and −209 mV vs SHE, which are split by 39 mV due to heme−heme electrostatic interactions in the maquette. These E_{m8} values are slightly more positive than the corresponding value for monoheme-$[\Delta 7\text{-His}]_2$, −222 mV, and diheme-$[\Delta 7\text{-His}]_2$, −188 and −238 mV.[14] In the case of Fe(DADPIX), only the electrochemistry of the mono-Fe(DADPIX) complex could be determined because of the weak second ferric Fe-(DADPIX) dissociation constant value, $K_{d2}^{Fe(III)}$. For mono-Fe(DADPIX)-$[\Delta 7\text{-H3m}]_2$, the increase in the ferrous Fe-(DADPIX) Soret absorption at 450 nm fits to an equilibrium midpoint reduction potential at pH 8, E_{m8}, value of -30 ± 10 mV vs SHE, as shown in Figure 8. The reduction potential of mono-Fe(DADPIX)-$[\Delta 7\text{-H3m}]_2$ is 160 mV (3.7 kcal/mol) more positive than mono-Fe(DADPIX)-$[\Delta 7\text{-H3m}]_2$. This 160 mV difference is similar to the 174 mV difference observed between the heme *b* and heme *a* maquettes, mono-Fe(PPIX)-$[H10A24]_2$ and mono-heme *a*-$[H10A24]_2$,[35] and the 140 mV positive shift in E_m observed upon conversion of a *c*-type heme vinyl group in *Thermus thermophilus* cytochrome c_{552} into a formyl group.[36] This similarity suggests that the two acetyl groups in Fe(DADPIX) impart the same electrochemical effect as the one formyl group in heme *a*. Furthermore, the data indicate that the majority of the electrochemical difference between natural heme *a* and heme *b* is due to the C-8 formyl substitutent.

Discussion

The $[\Delta 7\text{-H3m}]_2$ heme protein maquette has been utilized to evaluate the roles of electron-withdrawing groups on ferric and ferrous heme affinity and electrochemistry relevant to heme *a* in CcO. Fe(diacetyldeuterioporphyrin IX), Fe-(DADPIX), has been introduced into $[\Delta 7\text{-H3m}]_2$ to provide a synthetic analogue for the heme *a* electron-transfer cofactor in CcO. The thermodynamic affinity of the bis-imidazole heme binding sites in $[\Delta 7\text{-H3m}]_2$ for Fe(PPIX) and Fe-(DADPIX) were measured along with the related electrochemistry. Comparison of the coordination equilibria of Fe(PPIX)- and Fe(DADPIX)-$[\Delta 7\text{-H3m}]_2$ demonstrates that the electron-withdrawing acetyl groups on Fe(DADPIX) do not alter the ferrous affinity significantly but weaken the ferric affinity by 2500-fold relative to Fe(PPIX). This weakened ferric affinity results in the majority of the 160 mV positive shift in the reduction potential observed between Fe(DADPIX)-$[\Delta 7\text{-H3m}]_2$ and Fe(PPIX)-$[\Delta 7\text{-H3m}]_2$. These thermodynamic data suggest that one role of the electron-withdrawing C-8 formyl group on heme *a* is to raise the reduction potential by destabilizing the binding of the protein to the ferric state.

The incorporation of Fe(DADPIX) into designed heme proteins provides for the facile generation of synthetic analogues of heme *a*, the electron transfer heme cofactor in CcO. Previous studies on heme *a* incorporation into maquette scaffolds have demonstrated that porphyrin incorporation is relatively slow and can lead to significant changes in the

(35) Shifman, J. M.; Gibney, B. R.; Sharp, R. E.; Dutton, P. L. *Biochemistry*, **2000**, *39*, 14813−14821.
(36) Fee, J. A.; Todaro, T. R.; Luna, E.; Sanders, D.; Hunsicker-Wang, L. M.; Patel, K. M.; Bren, K. L.; Gomez-Moran, E.; Hill, M. G.; Ai, J.; Loehr, T. M.; Oertling, W. A.; Williams, P. A.; Stout, C. D.; McRee, D.; Pastuszyn, A. *Biochemistry*, **2004**, *43*, 12162−12176.

Scheme 1. Thermodynamic Analysis of Fe(PPIX) Affinity and Electrochemistry in the $[\Delta 7\text{-H3m}]_2$ Maquette Scaffold

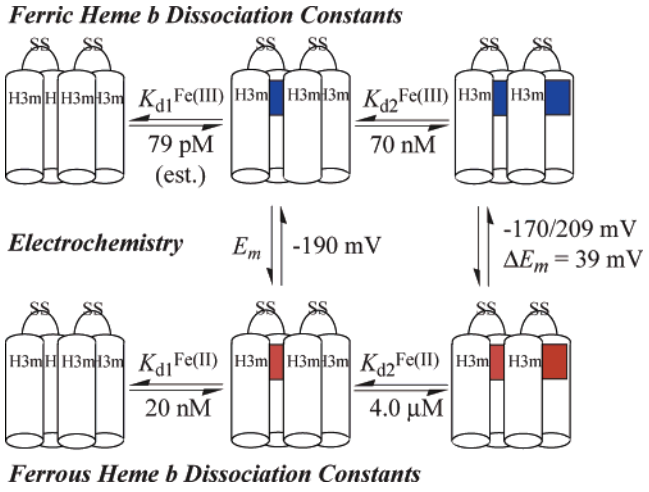

Scheme 2. Thermodynamic Analysis of Fe(DADPIX) Affinity and Electrochemistry in the $[\Delta 7\text{-H3m}]_2$ Maquette Scaffold

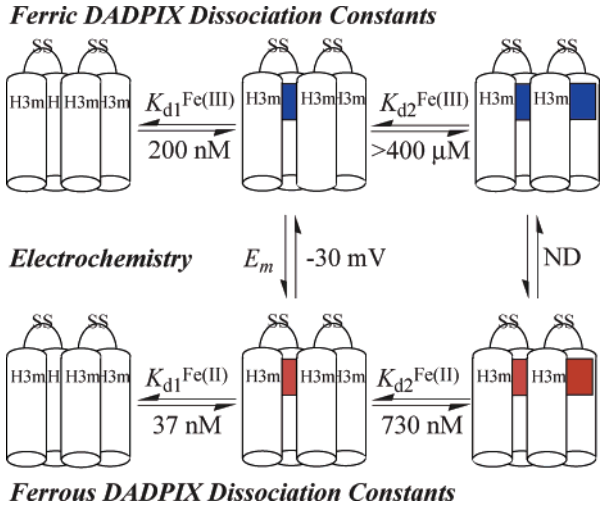

bundle structure.[5a] The data presented here demonstrate that use of Fe(DADPIX) provides for rapid incorporation of the heme cofactor (5 vs 90 min) with general retention of the bundle structure. These improvements are clearly due to the lack of the hydroxyethylfarnesyl chain whose hydrophobic character encourages porphyrin self-association. In addition, the use of Fe(DADPIX) provides spectroscopic and electrochemical characteristics that are similar to heme *a* bound to bis-His maquettes[8] and the low-spin bis-His site in CcO. As de novo heme protein design advances toward the construction of multicomponent redox proteins containing electron-transfer chains such as CcO maquettes,[5,8] the more positive reduction potentials observed for heme *a* and Fe(DADPIX) relative to Fe(PPIX) make them more attractive alternatives as electron acceptors.

Analysis of the coordination equilibrium of Fe(PPIX) binding to $[\Delta 7\text{-H3m}]_2$ presented in Scheme 1 provides detailed insight into the design of this heme protein maquette and demonstrates that similarities of the maquettes containing 3-methyl-L-histidine and L-histidine ligands. In the ferrous state, the data show that the second Fe(PPIX) binds 200-fold weaker than the first, dissociation constant values of 4 μM and 20 nM, respectively. Since the ferrous Fe(PPIX) core is formally neutral, i.e., $[Fe^{2+}(porphyrin^{2-})]^0$, with the charges on the propionates ignored because they are solvent-exposed, this 200-fold, or 3.1 kcal/mol, difference in heme binding is attributed to the steric hindrance of incorporating a second heme macrocycle in close proximity to the first within the protein scaffold.[14] In the ferric state, the binding of a second Fe(PPIX) is weakened by this steric hindrance, as well as an electrostatic repulsion due to the presence of another formally charged ferric Fe(PPIX) core, i.e., $[Fe^{3+}(porphyrin^{2-})]^{1+}$. The magnitude of this electrostatic repulsion is evidenced by the heme−heme electrostatic interaction of 39 mV, or 0.9 kcal/mol, observed in the electrochemistry of the diheme-bound state of Fe(PPIX)-$[\Delta 7\text{-H3m}]_2$. Based on these thermodynamic considerations, the dissociation constant of the first ferric Fe(PPIX), $K_{d1}^{Fe(III)}$ value, should be 885-fold, or 4.0 kcal/mol, tighter than the measured second ferric Fe(PPIX), $K_{d2}^{Fe(III)}$ value of 70 nM, or a $K_{d1}^{Fe(III)}$ value of 79 pM as reported in Scheme 1. The similarity of these data with those published for Fe(PPIX) binding to the L-histidine-containing maquette, Fe(PPIX)-$[\Delta 7\text{-His}]_2$, demonstrates that 3-methyl-L-histdine and L-histidine possess very similar Fe(PPIX) binding properties.[14]

Comparison of the thermodynamics of $[\Delta 7\text{-H3m}]_2$ binding to Fe(PPIX) and Fe(DADPIX) reveals both the steric and electronic consequences of porphyrin alteration on the affinity of the maquette scaffold for both oxidation states. In the ferrous state, the first dissociation constant for Fe(DADPIX) is 37 nM, a value only 1.9-fold, or 0.4 kcal/mol, weaker than that observed for Fe(PPIX) in this scaffold. Therefore, in terms of steric hindrance, the introduction of the bulkier acetyl substitutents has not greatly altered the affinity for the first ferrous heme. In addition, a comparison of the ratio of the second to first ferrous $K_d^{Fe(II)}$ values for Fe(PPIX) and Fe(DADPIX), 200 and 20, respectively, suggests that the acetyl groups of Fe(DADPIX) do not hinder the binding of the second Fe(DADPIX) to a larger extent than the vinyl groups of Fe(PPIX). However, in the oxidized state, significant changes in the ferric heme dissociation constants are observed between Fe(PPIX) and Fe(DADPIX), which are interpreted in terms of an electronic effect. The Fe(DADPIX) $K_{d1}^{Fe(III)}$ value is measured to be 200 nM, a value 2500-fold, or 4.6 kcal/mol, weaker than the corresponding value for Fe(PPIX), 79 pM. Thus, the acetyl groups significantly weaken the affinity of the bis-imidazole site for ferric heme iron. Caughey and co-workers have termed this a *cis*-effect,[37] since changes in the σ-donation abilities of the equatorial ligands, i.e., the porphyrin pyrrole pK_a values, alter the affinity of the metal for its axial ligands.[16]

As given in eq 1, the reduction potential of the bound heme is a function of the ratio of its ferric and ferrous heme dissociation constants. The elevation in the reduction potential of Fe(DADPIX)-$[\Delta 7\text{-H3m}]_2$ relative to Fe(PPIX)-$[\Delta 7\text{-H3m}]_2$ is a direct consequence of the changes in the ratio of the ferric and ferrous heme affinities described above.

(37) Caughey, W. S.; Barlow, C. H.; O'Keeffe, D. H.; O'Toole, M. C. *Ann. NY Acad. Sci.*, **1973**, *206*, 296−309.

The measured 4.6 kcal/mol weaker ferric affinity coupled with the 0.4 kcal/mol tighter ferrous affinity of Fe(DADPIX)-$[\Delta 7\text{-H3m}]_2$ compared to Fe(PPIX)-$[\Delta 7\text{-H3m}]_2$ indicates that a 4.2 kcal/mol, or 180 mV, change in the electrochemistry is expected. The observed 160 mV, or 3.7 kcal/mol, difference is as close as might be expected to the 180 mV value given the 0.5 kcal/mol error of the individual K_d and E_m measurements. Furthermore, the data in Schemes 1 and 2 indicate that destabilization of the ferric state by the electron-withdrawing acetyl groups is by far the major contributor to the rise in the reduction potential of Fe(DADPIX) relative to Fe(PPIX). The 160 mV difference in E_m between Fe(PPIX) and Fe(DADPIX) in $[\Delta 7\text{-H3m}]_2$ is similar to both the 140 mV positive shift in *Thermus thermophilus* cytochrome c_{552} upon incorporation of a formyl group and the 174 mV difference in reduction potential between Fe(PPIX) and heme *a* bound to a bis-His protein maquette, $[H10A24]_2$. Thus, the data suggest that the two acetyl groups in Fe(DADPIX) are as effective at adjusting the heme E_m value as one formyl group on heme *a*. This is likely due to the fact that both acetyl groups cannot conjugate into the porphyrin ring system simultaneously, which is evidenced in the structure of Ni(diacetyldeuterioporphyrin IX dimethyl ester) that shows one acetyl group rotated 17° from coincidence with the plane of its pyrrole ring.[38] Furthermore, the data suggest that one role of the formyl group on heme *a* is to raise the iron reduction potential by destabilizing the ferric state. Thus, a role of the hydroxyethylfarnesyl tail on heme *a* may be to compensate for weaker ferric heme affinity by providing a hydrogen bond donor[39] or by hydrophobic interactions so as to prevent heme loss during redox catalysis.

Conclusions

In summary, the thermodynamic analysis presented here indicates that electron-withdrawing groups on iron porphyrins serve to raise their reduction potentials by destabilizing the ferric ion affinity for axial imidazole ligands while leaving the ferrous affinities virtually unchanged. Given the chemical structure of heme *a* and its biosynthetic pathway from the more prevalent heme *b*, these data suggest that one role of the hydroxyethylfarnesyl tail at C-2 in heme *a* is to compensate for the loss in ferric axial ligand affinity due to electronic effects of the formyl group at C-8 by stabilizing the binding of both oxidation states. Future experiments with maquettes containing heme *o* are planned to evaluate the stabilization imparted by the C-2 farnesyl chain.[40]

Acknowledgment. We thank Dr. Masanori Sono for his assistance in the preparation of the bis-imidazole Fe(DADPIX) complex used in Figure 5A−D and Mr. Stephen Mui for assistance in the preparation of the TOC graphic. This work is supported by the grants from National Science Foundation (CHE-02-12884 to B.R.G.), the American Heart Association (0455900T to B.R.G.) and National Institutes of Health (GM 26730 to J.H.D.). J.H.A. is a NIH Biophysics trainee (T32 GM 08281). The resonance Raman spectrometer was funded by the University of Cincinnati. The analytical ultracentrifuge was purchased via a NIH Shared Instrumentation Grant (S10 RR 12848).

IC060072C

(38) Tamor, T. A.; Caughey, W. S.; Hoard, J. L. *J. Am. Chem. Soc.* 1965, *11*, 2305−2312.
(39) Wang, N.; Zhao, X.; Lu, Y. *J. Am. Chem. Soc.* **2005**, *127*, 16541−16547.
(40) Puustinen, A.; Wikström, M. *Proc. Natl. Acad. Sci., U.S.A.* **1991**, *88*, 6122−6126.
(41) Cheek, J.; Mandelman, D.; Poulos, T. L.; Dawson, J. H. *J. Biol. Inorg. Chem.* **1999,** *4*, 64−72.